2

Finger Vein Recognition

Kejun Wang, Hui Ma, Oluwatoyin P. Popoola and Jingyu Li
Pattern Recognition & Intelligent Systems Department, College of Automation,
Harbin Engineering University
China

1. Introduction

Smart recognition of human identity for security and control is a global issue of concern in our world today. Financial losses due to identity theft can be severe, and the integrity of security systems compromised. Hence, automatic authentication systems for control have found application in criminal identification, autonomous vending and automated banking among others. Among the many authentication systems that have been proposed and implemented, finger vein biometrics is emerging as the foolproof method of automated personal identification. Finger vein is a unique physiological biometric for identifying individuals based on the physical characteristics and attributes of the vein patterns in the human finger. It is a fairly recent technological advance in the field of biometrics that is being applied to different fields such as medical, financial, law enforcement facilities and other applications where high levels of security or privacy is very important. This technology is impressive because it requires only small, relatively cheap single-chip design, and has a very fast identification process that is contact-less and of higher accuracy when compared with other identification biometrics like fingerprint, iris, facial and others. This higher accuracy rate of finger vein is not unconnected with the fact that finger vein patterns are virtually impossible to forge thus it has become one of the fastest growing new biometric technology that is quickly finding its way from research labs to commercial development.
Historically, R&D at Hitachi of Japan (1997-2000) discovered that finger vein pattern recognition was a viable biometric for personal authentication technology and by 2000-2005 were the first to commercialize the technology into different product forms, such as ATMs. Their research reports false acceptance rate (FAR) of as low as 0.0001 % and false reject rate (FRR) of 0.1%. Today 70% of major financial institutions in Japan are using finger vein authentication.

Fig. 1. Hitachi of Japan history of research & development on finger-vein recognition technology

Fingerprints have been the most widely used and trusted biometrics. The reasons being: the ease of acquiring fingerprints, the availability of inexpensive fingerprint sensors and a long history of its use. However, limitations like the deterioration of the epidermis of the fingers, finger surface particles etc result in inaccuracies that call for more accurate and robust methods of authentication. Vein recognition technology however offers a promising solution to these challenges due the following characteristics. (1) Its universality and uniqueness. Just as individuals have unique fingerprints, so also they do have unique finger vein images. The vein images of most people remain unchanged despite ageing. (2) Hand and finger vein detection methods do not have any known negative effects on body health. (3) The condition of the epidermis has no effect on the result of vein detection. (4) Vein features are difficult to be forged and changed even by surgery [1]. These desirable properties make vein recognition a highly reliable authentication method.

Vein object extraction is the first crucial step in the process. The aim is to obtain vein ridges from the background. Recognition performance relates largely to the quality of vein object extraction. The standard practice is to acquire finger vein images by use of near-infrared spectroscopy. When a finger is placed across near infra-red light rays of 760 nm wavelength, finger vein patterns in the subcutaneous tissue of the finger are captured because deoxygenated hemoglobin in the vein absorb the light rays. The resulting vein image appears darker than the other regions of the finger, because only the blood vessels absorb the rays. The extraction method has a direct impact on feature extraction and feature matching [2]. Therefore, vein object extraction significantly affects the effectiveness of the entire system.

2. Processing

After vein image extraction, comes segmentation. The traditional vein extraction technology can be classified into three broad categories according to their approach to segmentation i.e separating the actual finder veins from the background and noise. There are those based on region information, those based on edge information, and those based on particular theories and tools. However, the application of the traditional single-threshold segmentation methods such as fixed threshold, total mean, total Otsu to perform segmentation, faces limitations in obtaining the desired accurate segmentation results. Using multi-threshold methods like local mean and local Otsu, improve these results but still cannot effectively deal with noise and over-segmentation effects [3], [4], [5], [6], [7],[8]. In a related research, reference [9] proposed an oriented filter method to enhance the image in order to eliminate noise and enhance ridgeline. Authors in [10] used the directionality feature of fingerprint to present a fingerprint image enhancement method based on orientation field. These two methods take the directionality characteristic of fingerprints into account, so they can enhance and de-noise fingerprint images effectively. Finger vein pattern also has textural and directionality features, with directionality being consistent within the local area. Inspired by methods in [9] and [10], we discuss in this chapter, finger vein pattern extraction methods using oriented filtering from the directionality feature of veins. These utilize the directionality feature of finger vein images using a group of oriented filters, and then extracting the vein object from an enhanced oriented filter image.

2.1 Normalization

Normalization is a pixel-wise operation often used in image processing. The main purpose of normalization is to get an output image with desirable mean and variance, which facilitates the subsequent processing. The uniformly illuminated image becomes normalized by this formula:

$$M = \frac{1}{M \times N} \sum_{i=0}^{M-1} \sum_{j=0}^{N-1} I(i,j) \tag{1}$$

$$VAR = \frac{1}{M \times N} \sum_{i=0}^{M-1} \sum_{j=0}^{N-1} (I(i,j) - M(I))^2 \tag{2}$$

$$G(i,j) = \begin{cases} M_0 + \sqrt{\frac{VAR_0}{VAR} \times (I(i,j) - M)^2}, I(i,j) \geq M \\ M_0 - \sqrt{\frac{VAR_0}{VAR} \times (I(i,j) - M)^2}, I(i,j) < M \end{cases} \tag{3}$$

Where M and VAR denote the estimated mean and variance of input image and $M_0 = 150$, $VAR_0 = 255$ are desired mean and variance values respectively. After normalization, the output image is ready for next processing step. The result of the above-mentioned process is shown in Fig.2. We note that Fig.2 image has lost some of its contrast but now has uniform illumination.

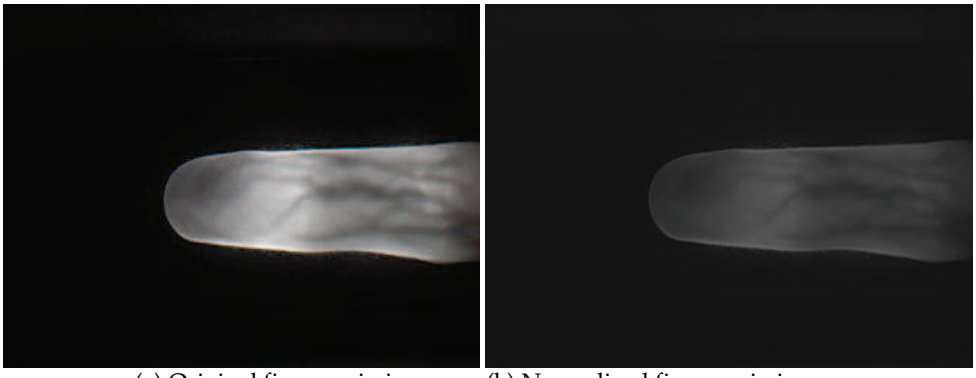

(a) Original finger vein image (b) Normalized finger vein image

Fig. 2. Original image and Normalized image

2.2 Oriented filter enhancement

Finger vein pattern has directionality characteristics, which the traditional filter methods do not take into account; therefore, its resultant filtering enhancement is not satisfactory. We propose a vein pattern extraction method using oriented filtering technology that takes into account the directionality feature of the veins. This algorithm utilizes a group of oriented filters to filter the image depending on the orientation of the local ridge.

a. Calculation of directional image

The directional image is an image transform, where we use the direction of every pixel of an image to represent the original vein image. Pixels' direction refers to the orientation of continuous gray value. We can determine the direction of pixel according to the gray distribution of the neighborhood. Pixels along the vein ridge have minimum gray level difference while pixels perpendicular to the vein ridge have the maximum gray level difference.

To estimate the orientation field of vein image, the direction of the vein is quantized into eight directions. Using a 9×9 template window as shown in Fig.2, we choose reference pixel $p(i,j)$ the center of the direction template. The values 1-8 of the template correspond to eight directions rotating from 0 to π. Each interval has and angle of $\pi/8$ in an anti-clockwise direction from the horizontal axis.

The main steps of the method are:

1. For every pixel, use the 9×9 rectangular window (shown as Fig.2) to obtain the pixel gray value average $\overline{M}_i$ $(i=1,2...8)$.
2. Divide $\overline{M}_i$ $(i=1,2...8)$ .into four groups. $\overline{M}_1$ and $\overline{M}_5$ are perpendicular in direction, so they belong to the same group. For the same reason, $\overline{M}_2$ and $\overline{M}_6$, $\overline{M}_3$ and $\overline{M}_7$, $\overline{M}_4$ and $\overline{M}_8$ belong to the same group. In each group, calculate ΔM - the absolute difference between two gray value averages $\overline{M}_j$ and $\overline{M}_{j+4}$.

$$\Delta M = \left|\overline{M_j} - \overline{M_{j+4}}\right|, j = 1,...,4 \tag{4}$$

   where j is the direction of the vein.
3. Choose the maximum ΔM to determine the pixel's possible directions $j_{\max}$ and $j_{\max}$ +4.
4. Determine the actual direction of $p(i,j)$ by comparing its gray value with the gray value averages of $j_{\max}$ and $j_{\max}$ +4. The closer value is its direction. Therefore, the pixels direction is given by:

$$D(x,y) = \begin{cases} j_{\max}, if \left|M - \overline{M}_j\right| < \left|M - \overline{M}_j + 4\right| \\ j_{\max} + 4, otherwise \end{cases} \tag{5}$$

When the above process is performed on each pixel in the image, we can obtain the directional image $D(x,y)$ of the vein image. Due to the presence of noise in the vein image, the estimated orientation field may not always be correct. In a small local neighborhood, the pixels' orientations are generally uniform; and so a local ridge orientation is specified for a block rather than at every pixel. Using a smoothing process on the point directional map, a continuous directional map is obtained. A continuous $w\times w$ window can be used to modify the incorrect ridge orientation and smooth the point directional map. The experiments show that w =8 is very good. We obtain each window's directional histogram and choose the peak value of the direction histogram as $P(x,y)$'s orientation. The continuous directional map $O(x,y)$ is defined as:

$$O(x,y) = ord(\max(N_i)) \tag{6}$$

7		6		5		4		3
8		7	6	5	4	3		2
		8				2		
1		1		$p(i, j)$		1		1
		2				8		
2		3	4	5	6	7		8
3		4		5		6		7

Fig. 3. 9×9 rectangular window

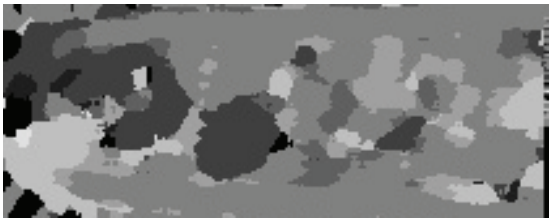

Fig. 4. Directional image of finger vein

Where $i = 1,2...8$, function $ord(*)$ is used to obtain the subscript of element *.

The directional image of finger vein is as shown in Fig.3 .Each color of directional image corresponds to a direction. As can be seen from the Fig.4, vein ridge has the feature of directionality, and the vein ridge orientation varies slowly in a local neighborhood.

b. Oriented filter

The vein directional image is a kind of textured pattern generated by using oriented filters based on directional map to enhance the original images. We designed eight filter masks, each one associated with the discrete ridge orientation of finger vein pixels. From the direction determined for a specific block (from the original image), a corresponding filter is selected to enhance this block image. The template coefficients of horizontal mask are designed first. To generate the seven other masks, the horizontal filter mask is rotated according to the direction of the vein. O'Gorman's rules for filter design which is described for enhancing fingerprint images consists of four key points:

1. An appropriate filter template size.
2. The width of the filter template should be odd in order that the template is symmetric in the direction of horizontal and vertical.
3. In the vertical direction, central part of the filter template coefficient should be positive while both sides of the coefficient negative.
4. The sum of all template coefficients should be zero.

Applying the above rules based on the direction of the finger vein, we modify the filter's coefficients so that they decay from the center to both ends of the template. The oriented filter's size is decided according to vein ridge width. From experiments, a filter template of size 7 has been shown to be quite effective.

$-c/3$	$-2c/3$	$-c$	$-c$	$-c$	$-2c/3$	$-c/3$
$b/3$	$2b/3$	b	b	b	$2b/3$	$b/3$
$a/3$	$2a/3$	a	a	a	$2a/3$	$a/3$
$d/3$	$2d/3$	d	d	d	$2d/3$	$d/3$
$a/3$	$2a/3$	a	a	a	$2a/3$	$a/3$
$b/3$	$2b/3$	b	b	b	$2b/3$	$b/3$
$-c/3$	$-2c/3$	$-c$	$-c$	$-c$	$-2c/3$	$-c/3$

(a) Template coefficient of horizontal oriented filter

–8	–16	–24	–24	–24	–16	–8
0	0	0	0	0	0	0
3	6	9	9	9	6	3
10	20	30	30	30	20	10
3	6	9	9	9	6	3
0	0	0	0	0	0	0
–8	–16	–24	–24	–24	–16	–8

(b) An example of oriented filter

Fig. 5. Template coefficient of horizontal oriented filter and an example of oriented filter

The coefficient spatial arrangement of the horizontal mask is shown in Fig.5.

a. The coefficients of the filter template should meet the following given conditions: $d+2a+2b-2c=0$, where $d>a>d\geq 0$, $c>0$; . An example of oriented filter is shown as Fig.5 (b). Now, aiming at every pixel (i,j) in the input image, we select a 3 neighborhood that takes (i,j) as the center. It is filtered with the mask that corresponds to the block orientation of the center (i,j) .This filtering technique is given by:

$$f(i,j)=\sum_{x=-3}^{3}\sum_{y=-3}^{3}G(i+x,j+y)g_{\theta}(x,y) \tag{7}$$

where (i,j) represents the pixel of original image, and x,y represents the size of oriented filter template and $g_{\theta}(x,y)$ represents the corresponding coefficients of the template. T_d represents the filtered image. It is possible that some gray values fall outside the [0, 255] range. Equation (8) is used to adjust the gray values to fall within the range.

$$f'(i,j)=Round(\frac{f(i,j)-f_{\min}(i,j)}{f_{\max}(i,j)-f_{\min}(i,j)}\times 255) \tag{8}$$

Where $f(i,j)$ represents the original gray of (i,j) , $f_{\min}(i,j)$ represents smallest gray value of original image, $f_{\max}(i,j)$ represents biggest gray value of original image, $f'(i,j)$ represents transformed gray of (i,j) and $Round(.)$ is a rounding function.

To generate the other seven masks, we rotate the horizontal filter mask according to the following equation: Where (i,j) represents the coordinates in the horizontal mask, and (i',j') represents the ones in the rotated mask.

$$\begin{bmatrix} i \\ j \end{bmatrix}=\begin{bmatrix} \cos\theta & \sin\theta \\ -\sin\theta & \cos\theta \end{bmatrix}\begin{bmatrix} i' \\ j' \end{bmatrix} \tag{9}$$

Where $\theta=(d-1)/\pi, d=1,2,...,8$, θ represents the rotation angel, and d represents the direction value of (i,j) .

To use this method, (i,j) is usually not an integer, so we need to use nearest neighbor interpolation to get the coefficients of the rotated mask. $g_{\theta}(i',j')$ (the coefficients in the rotated mask) is equal to $g_1(i,j)$ (the coefficients in the horizontal mask).

Suppose the four points (i_m, j_m), (i_m, j_n), (i_n, j_m), (i_n, j_n) compose a square centered at pixel (i, j), and $g_\theta(i_m, j_m)$, $g_\theta(i_m, j_m)$, $g_\theta(i_n, j_m)$, $g_\theta(i_n, j_n)$ are their corresponding coefficients in the horizontal mask, where $i_m < i < i_n$, $j_m < j < j_n$.
First, make interpolation between (i_m, j_n) and (i_n, j_n):

$$g(i, j_n) = g_1(i_m, j_n) + (i - j_m) \times [g_1(i_n, j_n) - g_1(i_m, j_n)] \tag{10}$$

Then make interpolation between (i_m, j_m) and α:

$$g(i, j_m) = g_1(i_m, j_m) + (i - i_m) \times [g_1(i_n, j_m) - g_1(i_m, j_m)] \tag{11}$$

Finally, make interpolation between a_0 and b_0:

$$g_\theta(i', j') = g(i, j_m) + (j - j_m) \times [g(i, j_n) - g(i, j_m)] \tag{12}$$

Once we have all eight filter masks, their coefficients can be used to enhance vein image.

2.3 Image segmentation

NiBlack segmentation method is a commonly used simple and effective local dynamic threshold algorithm, so we choose this method to segment the image. The basic idea of this algorithm is that for every pixel in the input image; calculate their mean and variance of its $r \times r$ neighborhood. Then the result of the following formula is used as threshold to segment image.

$$T(x, y) = m(x, y) + k \times s(x, y) \tag{13}$$

Fig. 6(a). Image enhanced by oriented filter

Fig. 6(b). Image after segmentation and noise removal

Where (x, y) represents pixel in the input image, $T(x, y)$ represents the threshold of $\forall\ a, a' \in M'$, $a = H(x) = T_d(T_\alpha(a_0))$ represents the mean value of $a_0 = T_\alpha^{-1}(T_d^{-1}(a))$'s $r \times r$ neighborhood, and $s(x, y)$ represents the standard deviation of $v(a') = v(a)$'s $a_0 = T_\alpha(v(a'))$ neighborhood, k is a correction coefficient. The experiments show that $v(a) = T_\alpha(v(a_0))$ equal to 9 and $v(a_0) = T_\alpha^{-1}(v(a'))$ equal to 0.01is excellent. There are some

small black blocks in the background and some small white holes on the target object in the segmented image. Such noise can be removed with area elimination method. Because of variability in image acquisition and the inherent differences in individual samples, the size and ratios of extracted finger veins are often inconsistent. In order to facilitate further research there is a need for standardization of the segmented vein image height (and width). The normalized image is shown in Fig.7. In the experiment, we have standardized the height of the image to 80 pixels.

Fig. 7. Standardized finger vein image width

Accurate extraction of finger vein pattern is a fundamental step in developing finger vein based biometric authentication systems. The finger vein pattern extraction method proposed and discussed above extends traditional image segmentation methods, by extracting vein object from the oriented filter enhanced image. The addition of oriented filter operation extracts smooth and continuous vein features from not only high quality vein images but also noisy low quality images and does not suffer from the over-segmentation problem.

3. Feature extraction, fusion and matching

Finger vein recognition as a feature for biometric recognition has excellent advantages such as being stable, contactless, unique, immune to counterfeiting, highly accurate etc. This makes finger-vein recognition widely considered as the most promising biometric technology for the future.

Naoto Miura [14] proposed one method for finger-vein recognition based on template matching. In the experiment, the finger-vein image is first binarized, and then using a distance transform noise is removed, and embedded hidden Markov model is used for finger-vein recognition. This approach is time intensive, and another major limitation is that it cannot recognize distorted finger-vein images correctly. Kejun Wang [15] combined wavelet moment, PCA and LDA transform for finger-vein recognition. Here the metric of finger-vein image is converted to a one-dimensional vector, which has been reduced dimensionally. To deal with the problem of high dimensionality, researchers usually first partition the finger-vein image and then principal component analysis (PCA) is applied. To date, this has been the most popular method for dimensionality reduction in finger-vein recognition research. Xueyan Li [16] proposed a method, which combines two-dimensional wavelet and texture characteristic, to recognize the finger vein while Xiaohua Qian [17] used seven moment invariant finger vein features. Euclidean distance and a pre-defined threshold were used as the classifying criterion for matching and recognition. Chengbo Yu [13] defined valley regions as finger vein features such that real features could not be missed and the false features would not be extracted. Zhongbo Zhang [18] proposed an algorithm based wavelet and neural network, which extracts features at multi-scale. Zhang's algorithm can capture features from degraded images.

3.1 Novel finger vein recognition methods based using fusion approach

The above-mentioned algorithms have different advantages for different problems in finger-vein recognition. However, because fingers have curved surfaces, finger vein diameter is not consistent and the texture characteristic is aperiodic. When near infrared light is used to acquire the image, the gray-scale is uneven and contrast is low; besides, finger veins are tiny and few in number, such that only very few features can be extracted. What is more, a change in the finger position can cause image translation and rotation and influence recognition negatively. To deal with these problems some novel fusion methods are used. First, we discuss a method based on relative distance and angle. This approach makes full use of the uniqueness of topology, the varied distances between the intersection points of two different vein images, and the differences in angles produced by these intersection points connections, all combined for recognition. This method overcomes the influence of image translation and rotation, because relative distance and angle don't change. Therefore, the method based on these identified characteristics has great use in practice.

3.1.1 Theoretical basis

Let a, b, and c be non-zero vectors. θ is the angle between two vectors, and the length of line segment is written as $\| a \|$.The thinned finger-vein image is illustrated as a function denoted as M, which is defined in field D ; where M is a subset of D. Image translation and rotation occurs in D. Image translation and rotation implies that every point of the image is translated by a vector and rotated by the some angle. The relative distances and angles remain constant before and after translation and rotation, which is proved as follows.

The topology produced by all the character point connections can be called the image M. Then M can be shown by the vectors: $a = \{a_0, a_1, ..., a_{n-1}\} \quad n \in N$.

Let $a[s] = \{a_s, a_{s+1}, ..., a_{s+n-1}\}$, were $a[s]$ denotes a vector a, translated by s unit distances.

If $g_s = < a, a[s] >$, where $< a, b >$ denotes the inner product of a and b; and $v(a) = (g_0, g_1, ..., g_{n-1})$, where $v(a)$ is the convolution of a.

Now after image M is translated by s unit distances in the plane D, we get the image $M' = M[s]$.

A random translation of image M is translated by T_d, is $T_d(a) = a[s]$,$(0 \le s \le n)$.

Theorem 1. Suppose T_d is a translation in D, then $v(a) = v(T(a))$.

Proof: $\forall\ s, t \in N$, there is

$$< a[t], a[s+t] > = < a, a[s] > \tag{14}$$

$$\exists \quad < a[t], a[s+t] >= \sum_i a_i[t] a_i[s+t] = \sum_i a_{i+t}[0] a_{i+t}[s] = \sum_i a_i[0] a_i[s] = < a[0], a[s] >$$

From formula (14), we know $\forall\ s, t \in N$, $\exists\ g_s(a[t]) = g_s(a)$ which satisfies

$$v(a[t]) = v(a) \tag{15}$$

For every T_d, $\exists\ T_d(a) = a(s)$ which leads to $v(a) = v(a[s]) = v(T(a))$.

Theorem 2. After transformation, the relative distances and angles produced by the character point connections are in unchanged

Proof: In the plane D, $\forall$ a_0 , b_0 , $c_0 \in M$ denotes the line segment vector produced by character point connections. θ_0 is the angle of a_0 and b_0. Any angle α, makes the image M rotate around its ordinate origin by α.
(α is positive while clockwise, and negative otherwise), which is a linear transform T_α. This results in image $\overline{M}$. For $\forall$ a and b, there is\

$$[a,b] = [a_0,b_0]\ T_\alpha = [a_0,b_0] \begin{bmatrix} \cos\alpha & \sin\alpha \\ -\sin\alpha & \cos\alpha \end{bmatrix} \tag{16}$$

Here $[a,b]$ is a homogeneous orthogonal rotated matrix, and $\|T_\alpha\| = \sqrt{\rho(T_\alpha^T T_\alpha)}$ =1, $\rho(\cdot)$ is the matrix radius. Then we can write

$$\|a\| = \sqrt{a^T a} = \sqrt{a_0^T T_\alpha^T T_\alpha a_0} = \|a_0\|.$$

Accordingly,

$$\| b \| = \| b_0 \| \tag{17}$$

$$< a,b > = < T_\alpha a_0, T_\alpha b_0 > = \|T_\alpha\|^2 < a_0, b_0 > = < a_0, b_0 >$$

This leads to $$\theta = \arccos \frac{< a,b >}{\|a\| \cdot \|b\|} = \theta_0 \tag{18}$$

Theorem 3. The relative distances and angles are invariable after the translation and rotation
Proof: Suppose the image M converts to M' after translation by T_d and rotation by T_α. $\forall$ $a, a' \in M'$, suppose $a = H(x) = T_d(T_\alpha(a_0))$, then $a_0 = T_\alpha^{-1}(T_d^{-1}(a))$. Suppose, too, $a' = T_\alpha^{-1}(a)$, then $a_0 = T_\alpha^{-1}(a')$.
From theorem 1, we know $v(a') = v(a)$, further because of $a_0 = T_\alpha(v(a'))$ and $v(a) = T_\alpha(v(a_0))$, so $v(a_0) = T_\alpha^{-1}(v(a'))$. All this leads up to

$$v(a_0) = v(H(a_0)) \tag{19}$$

3.1.2 Method description

Extract the intersecting points from the repaired thinned finger-vein image and connect all the points with each other. Compute the relative distances and angles to get the relative distance feature M, and the angle feature θ. Fuse these two features by "Logical And", and on this basis, match any two images to get the number of relative distances and angles that correlate. Only when both features are approximately the same, is the matching successful. Otherwise, the matching has failed.

A. Finger vein topology

Using Kejun Wang's method [19] for pre-processing hand-back vein image, combined with region merging and watershed algorithm, the finger-vein skeleton is extracted, thinned and further repaired. A fully meshed topology is formed by selecting the intersecting points on the thinned finger-vein image as character points and connecting these points to each other with straight lines, partitioning the image into several regions as shown in Fig.8.

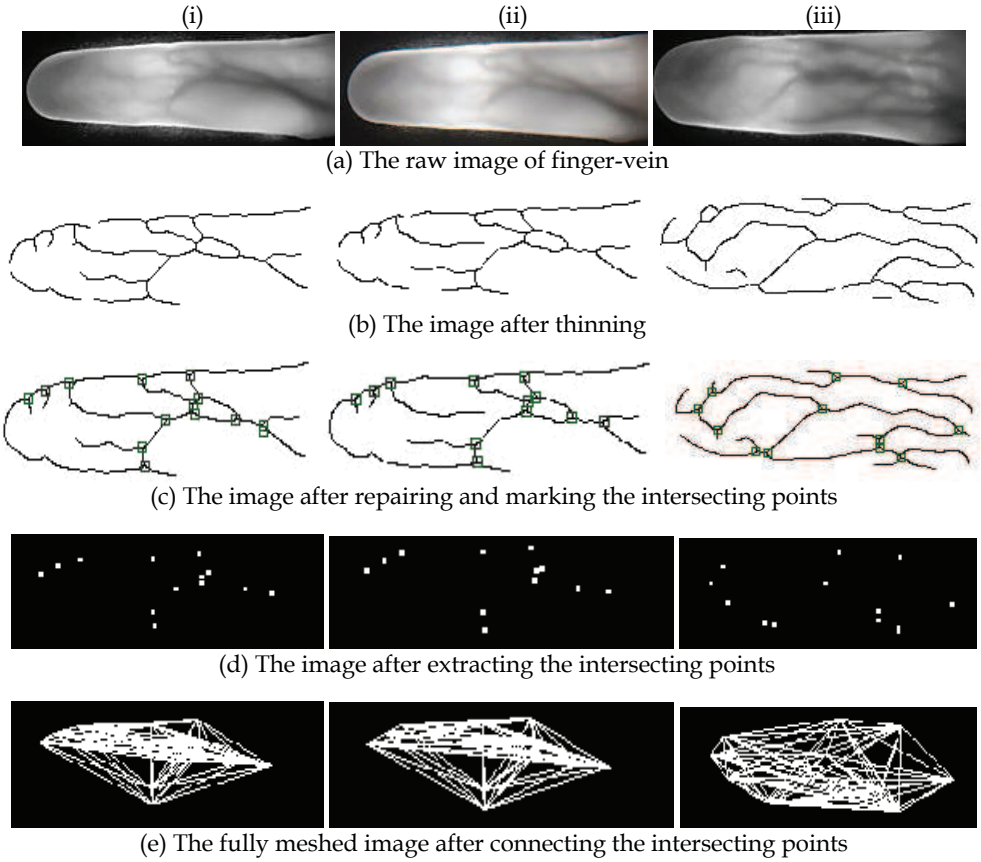

Fig. 8. The finger-vein image feature extraction process

In Fig.8, (i) and (ii) are two finger-vein images from same source, so their topology is similar. However, (iii) is of a different source and its topology is obviously different from (i) and (ii). Specifically, the topology expresses an integral property and peculiarity of finger-veins, the relationship between corresponding character points is of importance.

3.1.3 Matching finger-vein images using relative distance and angles

From the thinned finger-vein image of Fig.8 (b), we can see the random finger-vein pattern and inner structure. The inner characteristic points produced by the intersecting vein crossings reflect the unique property of the finger-vein. However, those breakpoints may be thought as finger-vein endpoints, which would influence recognition results. For this reason, the more reliable intersecting points are chosen to characterize finger-veins. Considering that different line segments are produced by intersecting points from different finger-vein images, the two features -relative distance and angle - are combined for matching.

Relative distance and angle are essential attributes of finger-veins, which ensure the feature uniqueness and reflect different characteristics of finger-vein structure. Fusion of the two

features with "Logical And" make the recognition results more reliable. Thus, matching two finger-vein images is converted into matching the similarity of topologies.
The detailed steps are as follows.

1. Calculate the relative distances and angles of finger-vein image. Suppose, there are d points of intersection in one image, then the number of relative distance is $d(d-1)/2$. The number of angles produced by the point connections is $d(d-1)(d-2)/2$. Here a set of finger-vein image features is defined as $R=(l_m,\theta_u)$, where l is the distance of any two intersecting points, θ is the angle produced by the point connections, m and u are the number index respectively. Suppose, $R_1=(l_m,\theta_u)$ and $R_2=(l_n,\theta_v)$ are two sets of finger-vein image features.
2. Compare m relative distances from R_1 with n relative distances from R_2, by calculating the number of approximately similar relative distances. If the number is greater than the pre-defined threshold, go to next step; else, the matching is assumed to have failed. To take care of position error of those points, we define $\| l_m - l_n \| < e$ to show the extent of similarity between any two Eigen values (e is the allowable error range). From experimental analysis, e =0.0005 is very appropriate.
3. Suppose there are q eigenvalues of approximately equivalent relative distances, connect the q character points in the two sets respectively, with each other. Thus, z angles are produced, which are denoted as θ_{z1} and θ_{z2} in R_1 and R_2 respectively. On this basis, calculate the number of approximately equivalent angles. If the number is greater than the pre-defined threshold, the matching is successful; else, the matching is thought to have failed. Similarly, $\| \theta_m - \theta_n \| < e'$ is used to show the relationship of two approximately equivalent. From experimental analysis, e' =0.006° is very appropriate.

3.2 Finger vein recognition based on wavelet moment fused with PCA transform

3.2.1 Finger vein feature extraction

Different people have different finger lengths. Also, there can be variation in the image captured for the same person due to positioning during the image capture process. Thus if image sizes are not standardized, there is bound to be representation error which leads to a decrease in the recognition rate. In this part, we resize the vein image into a specific image block size to facilitate further processing. The original image is standardized to a height of 80 pixels and split along the width into 80 × 80 sub-image block size. If the image is split evenly (given that the image width is generally about 200 pixels) there will be loss of information that will affect recognition. Therefore, the sub-blocks are created with an overlap of 60 pixels for every 80 × 80 image sub-block. The original image can thus be split into 6-7sub-images, with sufficient characteristic quantities for identification.
Set a matrix $A_{m\times n}$ to represent the standardized images $f(x,y)$.

$$A_{mn}=[A_0,A_1,A_2,...,A_{n-1}] \tag{20}$$

Which: A_i is a column vector, $i\in[0,n-1]$
Here we define the sub-block of the image width w, standardized image height h (in experiment w=*80*，h=*80*). Sub-images are extracted at interval r when (in this experiment r =*20*).

Thus can get sub-image matrix:

$$B_1 = [A_0, ..., A_{w-1}]$$
$$B_2 = [A_r, ..., A_{w-1+r}]$$
$$...$$
$$B_k = [A_{kr}, ..., A_{w-1+kr}]$$

[x] takes the maximum integer less than x .

$$k = \left[\frac{n-w}{r} + 1 \right] \tag{21}$$

Thus we get a total of $B_1, B_2, ..., B_k$ k sub- image, and the size of each sub-image is $w \times h$. Then we extract features for each sub-image B_i. The finger block, feature extraction and recognition process shown in Fig.12.

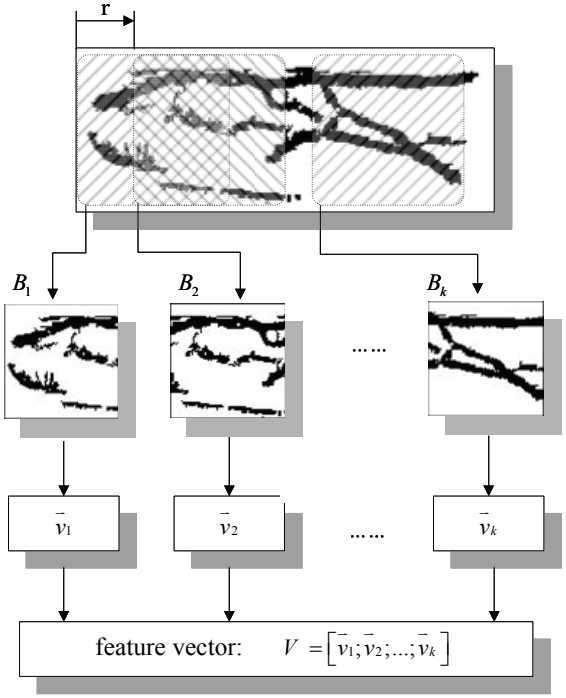

Fig. 12. The sketch map of sub-image extraction

3.2.2 Wavelet transform and wavelet moments extraction

Wavelet moment is an invariant descriptor for image features. A wavelet moment feature is invariant to image rotation, translation and scaling so it is successfully applied in the pattern recognition.

For each sub-image $B_i(x,y)$, its size is $w \times h$. Applying two dimensional Mallat decomposition algorithm, we can make wavelet decomposed image $B_i(x,y)$.

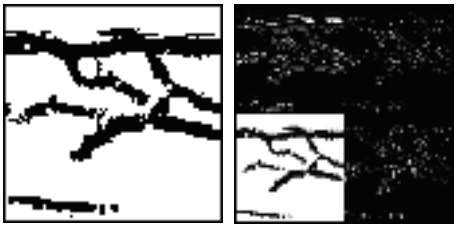

Fig. 13. The sub-image and result of wavelet decomposition

Setting $f(x,y) = B_i(x,y) \in L^2(R^2)$ to be the analyzed sub-image vein blocks, the wavelet decomposed layer is

$$f(x,y) = A_1 + D_1^1 + D_1^2 + D_1^3 \tag{22}$$

where A_1 is the scale for the low frequency component (i.e. approaching component), and D_1^1, D_1^2, D_1^3 are the scales for the horizontal, vertical and diagonal components respectively.

$$\begin{aligned} A_1 &= \sum_{(m,n)} c_1(m,n)\phi_1(m,n), \\ c_1(m,n) &= < f(x,y), \phi_1(m,n) > \end{aligned} \tag{23}$$

$$\begin{aligned} D_1^k &= \sum_{(m,n)} d_1^k(m,n)\psi_1^k(m,n), \\ d_1^k(m,n) &= < f(x,y), \psi_1^k(m,n) > \end{aligned} \tag{24}$$

Where $k = 1,2,3$ $c_1 = (m,n)$ is the coefficient of A_1
d_1^k is the coefficient of the three high frequency components.
$\phi_1(m,n)$ is the scale function
$\psi_1^k(m,n)$ is the wavelet function
Daub4 was chosen for wavelet decomposition, as it produced better identification results from several experimental compared with other wavelets. We use the approximation wavelet coefficients c_j to compute the wavelet moment [4]. Set $w_{p,q}$ expressed as (*p*+*q*) order central moments of $f(x,y)$. The wavelet moment approximation is:

$$\begin{cases} w_{p,q}^0 = 2^{-(p+q+1)j} \sum_{m,n \in Z} m^p n^q c_1(m,n) \\ w_{p,q}^k = 2^{-(p+q+1)j} \sum_{m,n \in Z} m^p n^q d_1^k(m,n) \end{cases} \tag{25}$$

Here we access the wavelet moment w_{22}.

3.2.3 PCA transformation

The advantage of using wavelet transform to reduce computation is explored here. Using each sub-image B_i directly without the PCA transform not only leads to poor classification of extracted features but also huge computational cost. After the low-frequency wavelet sub-

images compression of the original image to about one-fourth of the original size, PCA decomposition is applied on the sub-image which greatly reduces computation.

3.2.4 The transformation matrix

Here we analyze a layer of B_i wavelet decomposition of the low-frequency sub-image. For PCA, A_1 is transformed to a separate $wh/4$ dimension of image vector $\xi = Vec(A_1)$.

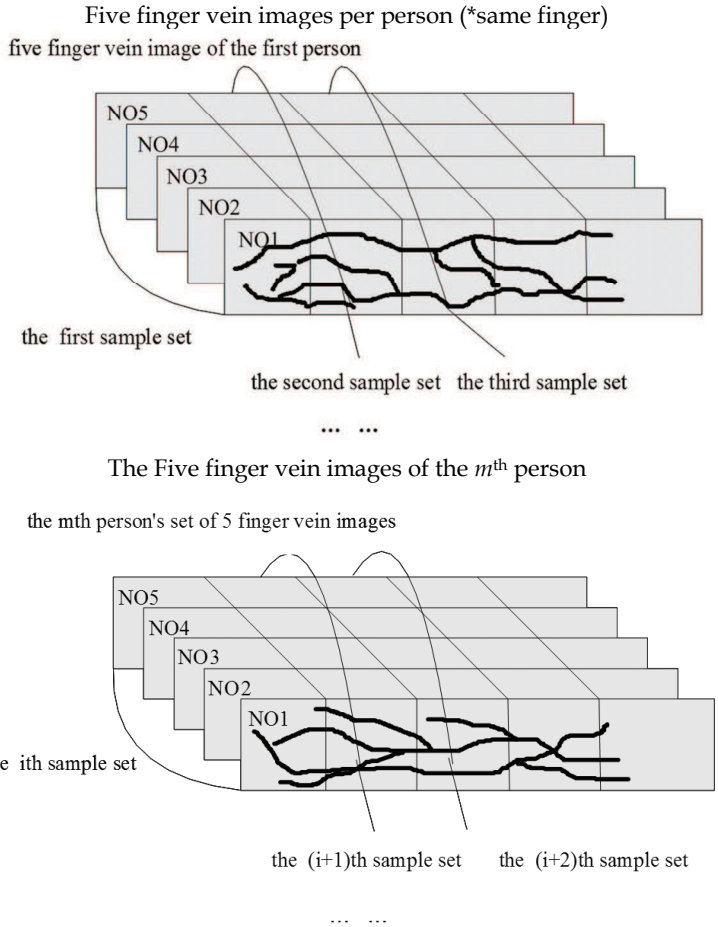

Fig. 14. The sketch map of sample classes after PCA transform

To illustrate the problem, we take finger vein samples from a total set of c people. Each sample of the same finger has five images as shown in Fig.14. (Note that Fig.14 is only for illustration purpose. In practice, there is an interval of 20pixels between two adjacent sub-blocks, and an overlap of 60pixels as earlier described).

The *n-th* sub-block set of the *m-th* person is indexed as $k_{m,n}$; where n = (1,2,3…., L) ; L_m is the total number of sub-blocks for person *m*.

To compare images we only use the $k_{\min}$ sub-image set where $k_{\min}$ = L = min $(L_1, L_2, L_3 ... L_m)$. when $k_{\min}$ = 5, then

$$k_{\min} = \min(k_{1,1}, k_{1,2}, ..., k_{1,5}, ..., k_{c,5}) \tag{26}$$

Thus, a total of $C = c \times k_{\min}$ of the available pattern classes, i.e. $\omega_1, \omega_2, ..., \omega_C$.
Four of the corresponding samples in the i-th class ($i = 5m + k$), $k = 1, 2, ...k_{\min}$ is the number of sub-image of each finger image, for simplicity, we write: $\xi_{i,1}, \xi_{i,2}, \xi_{i,3}, \xi_{i,4}, \xi_{i,5}$, and all are wh / 4 dimension column vectors. The total number of training samples is $N = 5C$.
Mean of the i-th class training sample:

$$\overline{\xi}_i = \frac{1}{5} \sum_{j=1}^{5} \xi_{i,j} \tag{27}$$

Mean of all training samples:

$$\overline{\xi} = \frac{1}{N} \sum_{i=1}^{C} \sum_{j=1}^{5} \xi_{ij} \tag{28}$$

The scatter matrix is:

$$S_t = \sum_{i=1}^{C} P(\omega_i)(\overline{\xi}_i - \overline{\xi})(\overline{\xi}_i - \overline{\xi})^T \tag{29}$$

where $P(\omega_i)$ is prior probability of the i-th class of training samples. Then we can obtain the characteristic value $\lambda_1, \lambda_2, ...,$ of S_1 (the value of these features have been lined up in sequence by order of $\lambda_1 \geq \lambda_2 \geq ...,$) and its corresponding eigenvector $\varphi_1, \varphi_2, ...,$. Take d before the largest eigenvalue corresponding to the standard eigenvectors orthogonal transformation matrix $P = [\varphi_1, \varphi_2, ..., \varphi_d]$. For each sub-image blocks B_i, through the wavelet decomposition of the low-frequency sub-image A_1, A_1 in accordance with the preceding method into a column vector ξ, to extract the features use the transformation matrix P obtained in the previous section, the following formula:

$$e = P^T \xi \tag{30}$$

This $e = [e_1, e_2, ..., e_d]$ is the PCA extraction of feature vectors from sub-image blocks. After several experiments, we found that when $d = 200$ we can get a good result, and when $d = 300$ i.e a 300-dimensional compression, we get the best recognition results.

3.2.5 LDA map

In general, PCA method is the best for describing feature characteristics, but not the best for feature classification. In order to get better classification results, we use the LDA method for further classification of PCA features.
Each sample is transformed into a lower d -dimensional space in the post-dimensional feature vector $e_i = [e_1^i, e_2^i, ..., e_d^i]$. Using PCA projection matrix P, $i = 1, 2, ..., N$ is the sample number. Our classifier design follows dimension reduction to get PCA feature vectors

$e_1, e_2, ..., e_N$ and form the class scatter matrix S_w and the within class scatter matrix S_b. Calculate the corresponding matrix $S_w^{-1}S_b$ of the l largest eigenvalue eigenvectors $\alpha_1, \alpha_2, ..., \alpha_l$. The l largest eigenvectors corresponding to the LDA transformation matrix $W_{LDA} = [\alpha_1, \alpha_2, ..., \alpha_l]$. Then we use the LDA transformation matrix W_{LDA} as

$$z_i = [z_1^i, z_2^i, ..., z_l^i] = W_{LDA}^T e_i \quad , i = 1, 2, ..., N \text{ is the sample number.} \tag{31}$$

Thus, we can use the best classification feature z vector to replace the feature vectors e for identification and classification.

3.2.6 Matching and recognition

Through the above wavelet decomposition and PCA transform for each sub-image B_i, we obtain wavelet moments w_{22} and extract feature vector z of PCA and LDA. B_i is characterized by $v_i = [w_{22}; z]$. Matching feature vectors of finger1 $v_i = [w_{22}; z]$ and of finger 2 can be done as follows.

The first step is the length of V and V' and may not be the same, that is, k and k' is not necessarily the same. Here we define:

$$K = \min(k, k') \tag{32}$$

Taking the K vectors of V and V' for comparison, first analyze the corresponding sub-image blocks v_i and v'_i.

$$v_i = [w_{22}; z] \ , \ v'_i = [w'_{22}; z'] \tag{33}$$

From several experiments, we set two threshold vectors w_t z_t. Euclidean distance between B_i sub-images, δ_i is defined for two feature vectors w and w' from V and V'. A matching score defined for V and V' feature w_{22} of wavelet moment of corresponding sub-image B_i matching score:

$$w\_mark_i = \begin{cases} \dfrac{w_t - \delta_i}{w_t} & if \quad \delta_i < w_t \\ 0 & else \end{cases} \tag{34}$$

Finally, we obtain wavelet moment feature of the finger matching score:

$$w\_mark = \sum_{i=0}^{K} w\_mark_i \tag{35}$$

Similarly, we create a match V and V', of the feature vector z scores z_mark.

Finally, combining the scores:

$$total\_mark = s_1 \times w\_mark + s_2 \times z\_mark \tag{36}$$

s_1, s_2 are the share of feature matching scores, and $s_1 \geq 0, s_2 \geq 0, \ s_1 + s_2 = 1$.

Thus, if the finger vein 1 and 2 match $total\_mark$ value score is greater than a given threshold, the two fingers match, otherwise they do not match. A minimum distance classifier can also be used for the recognition task.

4. Experimental results

4.1 Processing experimental results

To verify the effectiveness of the proposed method, we test the algorithm using images from a custom finger vein image database. The database includes five images each of 300 individuals' finger veins. Each image size is 320*240.

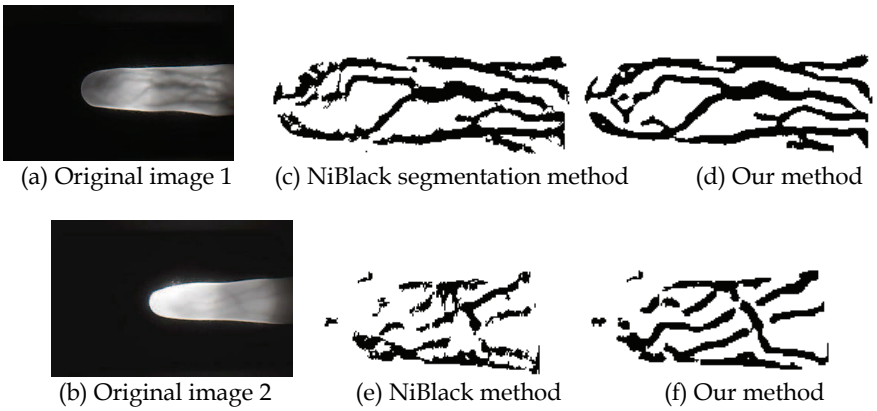

(a) Original image 1 (c) NiBlack segmentation method (d) Our method

(b) Original image 2 (e) NiBlack method (f) Our method

Fig. 15. Experimental results

We have used a variety of traditional segmentation algorithms and their improved algorithms to segment vein image. But segmentation results of vein image by these algorithms aren't ideal. Because the result of NiBlack segmentation method is better than other methods [13], we use NiBlack segmentation method as the benchmark for comparison. Segmentation was done for all the images in our database using NiBlack segmentation method and using our method. Experimental results show that our method has better performance. To take full account of the original image quality factor, we select two typical images from our database with one from high quality images and the other from poor quality images to show the results of comparative test. Where Fig. 15(a) is the high-quality vein image in which veins are clear and the background noise is small. Fig. 15(b) is the low-quality vein image. The uneven illumination caused the finger vein image to be fuzzy, which seriously affects image quality. We extract veins feature by using our method and compare with results of the NiBlack segmentation method. Experimental results shown in Fig. 15(c) and Fig. 15(e) are obtained from the NiBlack method applied in [9]. This algorithm extracts smooth and continuous vein features of high-quality image. There are a few pseudo-vein characteristics in Fig. 15(c). But in Fig. 15(e), there is much noise in the segmentation results. Segmented image features have poor continuity and smoothness, and there is the effect of the over-segmentation. Experimental results show that apart from smoothness and continuity or removal of noise and pseudo-vein characteristics, the method proposed in this paper extracts vein features effectively not only from the high-quality

images but also from the low-quality vein images as shown in Fig.15(d) and Fig.15(f). We show that the algorithm proposed in this paper performs better than the traditional NiBlack method.

4.2 Relative distance and angle experimental results

Finger-vein images (size 320×240) of 300 people were selected randomly from Harbin Engineering University finger-vein database. One forefinger vein image of each person was acquired, so there are 300 training images.

Generally, a good recognition algorithm can be successfully trained on a small dataset to get the required parameters and achieve good performance on a large test dataset. Therefore four more images from the forefinger of those 300 people were acquired giving a total sum of 1200 images to be used as verification dataset.

When matching, every sample is matched with others, so there are (300×299)/2 = 44850 matching times; 300 of which are legal, while the others are illegal matches. Two different verifying curves are shown in Fig.16. The horizontal axis stands for the matching threshold, and vertical axis stands for the corresponding probability density. The solid curve is legal matching curve, while the dashed is illegal. Both curves are similar to the Gaussian distribution. The two curves intersect, at a threshold of 0.41. The mean legal matching distance corresponds to the wave crest near to 0.21 on the horizontal axis, and the mean of illegal matching distance corresponds to the wave crest near to 0.62 on the horizontal axis. The two wave crests are far from each other with very small intersection. So this method can recognize different finger-veins, especially when the threshold is in the range [0.09-0.38], where the GAR is highest.

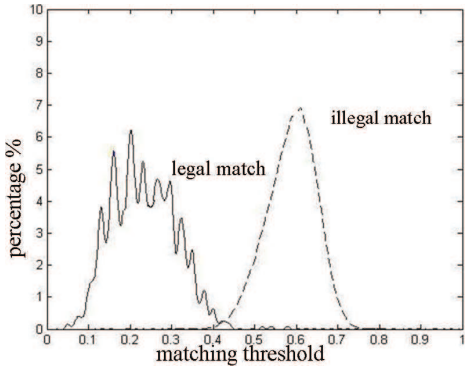

Fig. 16. Legal matching curve and illegal matching curve

The relationship between FRR and FAR is shown in Fig.17. For this method, the closer the ROC curve is to the horizontal axis, the higher the Genuine Acceptance Rate (GAR). Besides, the threshold should be set suitably according to the fact, when FRR and FAR are equivalent, the threshold is 0.47, that is to say, EER is 13.5%. In this case, GAR of the system is 86.5%. The result indicates that this method is reasonable, giving accurate finger-vein recognition.

The method above compares the numbers of relative distances and angles which are approximately equivalent from two finger-vein images. In the second step, only the

intersecting points which are matched successfully on the first step are used and thus, computation of superfluous information is avoided and only information vital to decision making is used. Only when the two matching steps are successful is the recognition successful. According to Theorem 3, the relative distance and angle would not change when even after image translation and rotation. So the proposed algorithm is an effective method for finger-vein recognition.

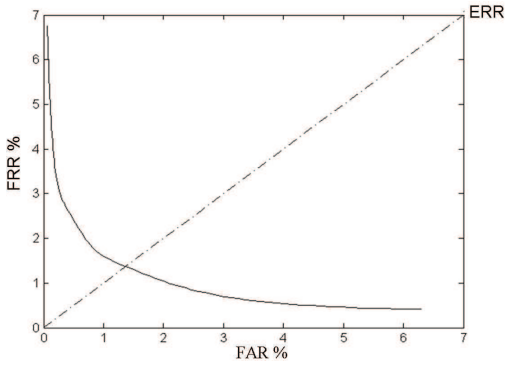

Fig. 17. ROC curve of the method

In 1:1 verifying mode, compare the one image out of 1200 samples in verifying set with the image, which has the same source with the former one, in training set to verify. The experiment result is shown in Tab.1, the times of success are 1120, and the rate of success is 93.33%. In 1:n recognition mode, compare the 1200 images with all images in training set, 360000 times in sum. The result is as Tab.2, the times of FAR is 25488, and GAR is 92.92%.

Total matching times	Number of successes	Number of failures	Success rate (%)	FRR(%)
1200	1120	80	93.33	6.67

Table 1. Test result of FRR in 1:1 mode

Total matching times	Total false acceptance	GAR (%)	FAR(%)
360000	25488	92.92	7.08

Table 2. Test result of FAR in 1:n mode

To test the ability to overcome image translation and rotation, translate randomly in the range $[-10,+10]$ and rotate the image randomly in the range $[-10^0,+10^0]$, in order to establish the translation and rotation test sets. Then verify and recognize the two sets respectively. The samples which have the same source are compared in a 1:1 experiment; matching each sample from the two sets with the samples from the training set to accomplish 1:n experiment. The result is shown in Tab.3, Tab.4, Tab.5 and Tab.6.

	Total matching times	Number of successes	Number of failures	Success rate (%)	FRR(%)
1:1	1200	1111	89	92.58	7.42

Table 3. Translation test set verification result (1:1)

	Total matching times	No. of genuine acceptance	GAR(%)	FAR(%)
1:n	360000	27900	92.25	7.75

Table 4. Translation test set recognition result (1:n)

As the experiment shows, in 1:1 mode the rate of success can reach 92.58% even though the finger-vein image is translated, and can reach 91.75% when rotated. In 1: n mode, GAR can reach 92.25% and 91.17% respectively, which implies a robust recognition system. Further, the method can overcome the influence caused by image translation and rotation, thus it can meet practical requirements.

	Total matching times	Number of successes	Number of failures	Success rate (%)	FRR(%)
1:1	1200	1101	99	91.75	8.25

Table 5. Rotation test set verification result (1:1)

	Total matching times	No. of genuine acceptance	GAR(%)	FAR(%)
1:n	360000	31788	91.17	8.83

Table 6. Rotation test set recognition result (1:n)

4.5.5 Experimental results analysis

The algorithm was implemented on a Windows XP platform using Visual C + +6.0. Finger vein image capture was performed taking into account the convenience of users, while collecting index finger and middle finger vein images. A total of 287 finger vein images collected for each finger 5 times, and in all, a total of 287x5 = 1435 were collected to form finger vein library. Two sets 287 x 2 = 574 were taken for verification.

The identification results based on template matching:

We first according to the method proposed in reference [1], recognition for the veins of our library of images. In 1:1 verification mode, we use the validation library of 574 samples to verify the experimental results shown in Tab.7.

Matching times	Pass times	Reject recognition times	Correct recognition rate (%)	Reject recognition rate (%)
574	559	15	97.4	2.6

Table 7. The results of refusing ratio of 1:1

For 1: n identification model, we use the validation library to identify 574 samples of the experimental results shown in Tab.8.

Matching times	False recognition times	False recognition rate (%)
574	7	1.2

Table 8. The result of mistaken identifying ratio of 1: n

For a number of reasons, we realize that the algorithm recognition rate is not as high as the reference [1], perhaps due to the acquisition of image and acquisition machine quality problems.

The identification results based on wavelet moment:

We first decompose the predetermined wavelet sample in the vein sample database, and then construct the wavelet moment features using identified wavelet coefficients.

A few typical experimental results of 1:1 verification mode shown in Tab.9.

	Matching times	Pass times	Reject recognition times	Correct recognition rate (%)	Reject recognition rate (%)
Hear	574	536	38	93.4	6.6
Daub4	574	547	27	95.3	4.7
Daub8	574	543	31	94.6	5.4
coif2	574	534	40	93.04	6.96
sym	574	529	45	92.2	7.8

Table 9. The results of rejection ratio with different wavelet base in the 1:1 case

For 1: n identification pattern, the experimental results shown in Tab.10.

	Matching times	False recognition times	false recognition rate
Haar	574	27	4.7
Daub4	574	11	1.9
Daub8	574	19	3.3
coif2	574	30	5.2
sym	574	33	5.7

Table 10. Results of mistaken identifying with different wavelet base in the case of 1: n

We chose Daub4 to carry out wavelet decomposition, identification was better than other wavelets.
Identification results of wavelet moment integration of PCA.
When PCA is used for dimension reduction, the relationship of selection of the compressed dimension k and the proportion of it represent components shown in Tab.11:

$$w_k = \sum_{i=1}^{k} \lambda_i / \sum_{i=1}^{N} \lambda_i \tag{37}$$

k	215	240	276	299	338	368	380	392
w_k	0.75	0.80	0.86	0.90	0.95	0.98	0.99	1.00

Table 11. The compressed dimension and it's proportion

To balance computation and weighting, we use 300 as the dimension for decomposition. Authentication in 1:1 mode and 1: n identification pattern, we use 574 samples in the validation library for the experimental, results shown in Tab.12, 13.

Matching times	Pass times	reject recognition times	recognition rate (%)	reject recognition rate (%)
574	568	6	98.95	1.05

Table 12. Results of rejection ratio of 1:1

Matching times	False recognition times	False recognition rate (%)
574	4	0.7

Table 13. The results of mistaken identifying ratio of 1: n

As seen from the recognition results, recognition rate and rejection rate in the method based on wavelet PCA can meet the requirements of practical applications. In recognition speed, that is, 1: n of the mode can meet the requirements.

5. Conclusion

Accurate extraction of finger vein pattern is a fundamental step in developing finger vein based biometric authentication systems. Finger veins have textured patterns, and the directional map of a finger vein image represents an intrinsic nature of the image. The finger vein pattern extraction method using oriented filtering technology. Our method extends traditional image segmentation methods, by extracting vein object from the oriented filter enhanced image. Experimental results indicate that our method is a better enhancement over the traditional NiBlack method [11], [12], [13], and has good segmentation results even with low-quality images. The addition of oriented filter operation, extracts smooth and continuous vein features not only from high quality vein images but also handles noisy low quality images and does not suffer from the over-segmentation problem. However, it requires a little more processing time because of the added oriented filter operation.

Topology is an essential image property and usually, even an inflection point may contain plenty of accurate information. Finger-vein recognition is faced with some basic challenges, like positioning, the influence of image translation and rotation etc. To address these problems, essential topology attributes of individual finger veins are utilized in a novel method. Particularly, the relative distance and angles of vein intersection points are used to characterize a finger-vein for recognition, since the topology of finger-vein is invariant to image translation and rotation. The first step is to extract those intersecting points of the thinned finger-vein image, and connect them with line segments. Then relative distances and angles are calculated. Finally combine the two features for matching and recognition. Experimental results indicate that the method can accurately recognize finger-vein, and to a certain degree, overcome the influence image translation and rotation. Furthermore, the method resolves the difficult problem of finger-vein positioning. It is also computationally efficient with minimal storage requirement, which makes the method of practical significance. However there are still problems of non- recognition and false recognition. Besides, pre-procession is an import requirement for this method and the accuracy of pre-processing influences recognition result significantly. In view of this, further research will be done on the pre-procession method, to improve the image quality and the accuracy of feature extraction, and subsequently improve system reliability.

This chapter discussed recent approaches to solving the problem of varying finger lengths and proposed using a set of images of same size interval in a selected sub-block approach. For each image sub-block, wavelet moment was performed and PCA features extracted. LDA transform is performed, and the two features were combined for recognition. For

matching and identification, we proposed a method of fuzzy matching scores. Experimental results show that wavelet moment PCA fusion method achieved good recognition performance; error rate FAR was 0.7%, rejection rate FRR of 1.05%. In future research, we are committed to further study finger vein feature fusion with fingerprint and other features to improve system reliability.

6. References

[1] N. Miura, A. Nagasaka and T. Miyatake, Extraction of finger-vein patterns using maximum curvature points in image profiles, *IEICE Trans. Inf. & Syst*. Vol.90, no.D(8),pp. 1185-1194, 2007.

[2] Shahin M, Badawi A, Kamel M. Biometric authentication using fast correlation of near infrared hand vein patterns, *J. International Journal of Biometrical Sciences*, vol.2,no.3,pp.141-148,2007.

[3] Lin Xirong,Zhuang Bo,Su Xiaosheng, ZhouYunlong, Bao Guiqiu. Measurement and matching of human vein pattern characteristics, *J.Journal of Tsinghua University (Science and Technology)*.vol. 43no. 2 pp.164-167, 2003. (In Chinese.)

[4] H.Tian, S.K.Lam, T. Srikanthan. Implementing OTSU's Thresholding Process Using Area-time Efficient Logarithmic Approximation Unit, *J. Circuits And Systems*, vol.5, pp. 21-24, 2003.

[5] Zhongbo Zhang, Siliang Ma, Xiao Han. Multiscale Feature Extraction of Finger-Vein Patterns Based on Curvelets and Local Interconnection Structure Neural Network, *IEEE Proceedings of the 18th International Conference on Pattern Recognition (ICPR'06)*, Hong Kong, China,vol 4, pp.145-148,2006.

[6] M.Naoto, A.Nagasaka, iM.Takafm Feature Extraction of Finger-vein Patterns Based on Repeated Line Tracking and Its Application to Personal Identification, *J. Machine Vision and Application*, vol. 15, no.4, pp. 194-203, 2004.

[7] Rigau J. Feixas, M.Sbert. Metal Medical image segmentation based on mutual information maximization, *In Proceedings of MICCAI 2004, Saint-Malo, France pp.*135-142, 2004.

[8] Yuhang Ding, Dayan Zhuang and Kejun Wang, A Study of Hand Vein Recognition Method, Mechatronics and Automation, *2005 IEEE International Conference*, vol. 4 no.29pp.2106–2110, 2005.

[9] O'Gorman, L. Lindeberg, J.V. Nickerson. An approach to fingerprint filter design, *Pattern Recognition*, vol. 22 no.1pp. 29-38, 1989.

[10] Xiping Luo; Jie Tian. Image Enhancement and Minutia Matching Algorithms in Automated Fingerprint Identification System, *J Journal of Software*, vol. 13 no.5pp. 946-956. 2002. (In Chinese.)

[11] W. Niblack. *An Introduction to Digital Image Processing*, Prentice Hall, ISBN 978-0134806747, Englewood Cliffs, NJ, pp.115-116, 1986

[12] Kejun Wang Zhi Yuan. Finger vein recognition based on wavelet moment fused with PCA transform, *J Pattern Recognition and Artificial Intelligence*, vol. 20 no.5 pp. 692-697, 2007. (In Chinese.)

[13] Chengbo Yu, Huafeng Qing, *Biometric Identification Technology Finger Vein Identification Technology*: Tsinghua University Press, 2009, pp: 81-87. (In Chinese.)

[14] Naoto Miura, Akio Nagasaka, Takafumi Miyatake. Feature extraction of finger-vein patterns based on repeated line tracking and its application to personal identification [J]. *Machine Vision and Applications*, 2004,15(4):194 -203

[15] Kejun Wang, Yuan Zhi. Finger Vein Recognition Based on Wavelet Moment Fused with PCA Transform. [J] *Pattern Recognition and Artificial Intelligence*. 2007

[16] Xueyan Li. Study of Multibiometrics System Based on Fingerprint and Finger Vein[D]. the doctorate dissertations of Jilin University. 2008.

[17] Xiaohua Qian. Research of Finger-vein Recognition Algorithm[D]. MA Dissertation of Jilin University. 2009.

[18] Zhong Bo Zhang, Dan Yang Wu, Si Liang Ma. Pattern Recognition, 2006. ICPR 2006. 18th International Conference on Volume: 4 Digital Object Identifier: 10.1109/ICPR.2006.848. Publication Year: 2006, Page(s): 145 – 148

[19] Kejun Wang, Yuhang Ding, Dazhen Wang. A Study of Hand Vein-based Identity Authentication Method [J]. *Science & Technology Review*. 2005, 23(1) :35-37.

[20] Ji Hu, SunJixiang, YaoWei. Wavelet Moment for Images. *Journal of Circuits and Systems*, 2005, 10(6):132-136 (inChinese)

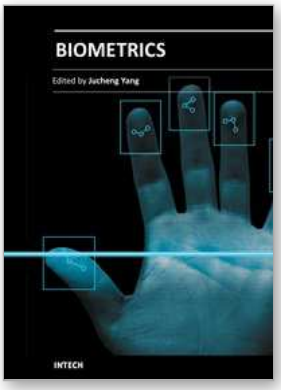

Biometrics

Edited by Dr. Jucheng Yang

ISBN 978-953-307-618-8
Hard cover, 266 pages
Publisher InTech
Published online 20, June, 2011
Published in print edition June, 2011

Biometrics uses methods for unique recognition of humans based upon one or more intrinsic physical or behavioral traits. In computer science, particularly, biometrics is used as a form of identity access management and access control. It is also used to identify individuals in groups that are under surveillance. The book consists of 13 chapters, each focusing on a certain aspect of the problem. The book chapters are divided into three sections: physical biometrics, behavioral biometrics and medical biometrics. The key objective of the book is to provide comprehensive reference and text on human authentication and people identity verification from both physiological, behavioural and other points of view. It aims to publish new insights into current innovations in computer systems and technology for biometrics development and its applications. The book was reviewed by the editor Dr. Jucheng Yang, and many of the guest editors, such as Dr. Girija Chetty, Dr. Norman Poh, Dr. Loris Nanni, Dr. Jianjiang Feng, Dr. Dongsun Park, Dr. Sook Yoon and so on, who also made a significant contribution to the book.

How to reference

In order to correctly reference this scholarly work, feel free to copy and paste the following:

Kejun Wang, Hui Ma, Oluwatoyin P. Popoola and Jingyu Liu (2011). Finger vein recognition, Biometrics, Dr. Jucheng Yang (Ed.), ISBN: 978-953-307-618-8, InTech, Available from: http://www.intechopen.com/books/biometrics/finger-vein-recognition

INTECH
open science | open minds

InTech Europe
University Campus STeP Ri
Slavka Krautzeka 83/A
51000 Rijeka, Croatia
Phone: +385 (51) 770 447
Fax: +385 (51) 686 166
www.intechopen.com

InTech China
Unit 405, Office Block, Hotel Equatorial Shanghai
No.65, Yan An Road (West), Shanghai, 200040, China
中国上海市延安西路65号上海国际贵都大饭店办公楼405单元
Phone: +86-21-62489820
Fax: +86-21-62489821